JACS
JOURNAL OF THE AMERICAN CHEMICAL SOCIETY

ARTICLE

pubs.acs.org/JACS

Three Dimensional Models of Cu^{2+}-Aβ(1−16) Complexes from Computational Approaches

Jorge Alí-Torres, Jean-Didier Maréchal,* Luis Rodríguez-Santiago, and Mariona Sodupe*

Departament de Química, Universitat Autònoma de Barcelona, 08193 Bellaterra, Barcelona, Spain

Supporting Information

ABSTRACT: Elucidation of the coordination of metal ions to Aβ is essential to understand their role in its aggregation and to rationally design new chelators with potential therapeutic applications in Alzheimer disease. Because of that, in the last 10 years several studies have focused their attention in determining the coordination properties of Cu^{2+} interacting with Aβ. However, more important than characterizing the first coordination sphere of the metal is the determination of the whole Cu^{2+}-Aβ structure. In this study, we combine homology modeling (HM) techniques with quantum mechanics based approaches (QM) to determine plausible three-dimensional models for Cu^{2+}-Aβ(1−16) with three histidines in their coordination sphere. We considered both ε and δ coordination of histidines 6, 13, and 14 as well as the coordination of different possible candidates containing oxygen as fourth ligand (Asp1, Glu3, Asp7, Glu11, and CO_{Ala2}). Among the 32 models that enclose COO^-, the lowest energy structures correspond to $[O^{E3},N_\delta^{H6},N_\varepsilon^{H13},N_\varepsilon^{H14}]$ (**1**), $[O^{E3},N_\delta^{H6},N_\delta^{H13},N_\delta^{H14}]$ (**2**), and $[O^{D7},N_\varepsilon^{H6},N_\delta^{H13},N_\delta^{H14}]$ (**3**). The most stable model containing CO_{Ala2} as fourth ligand in the Cu^{2+} coordination sphere is $[O_c^{A2},N_\varepsilon^{H6},N_\delta^{H13},N_\varepsilon^{H14}]$ (**4**). An estimation of the relative stability between Glu3 (**1**) and CO_{Ala2} (**4**) coordinated complexes seems to indicate that the preference for the latter coordination may be due to solvent effects. The present results also show the relationship between the peptidic and metallic moieties in defining the overall geometry of the complex and illustrate that the final stability of the complexes results from a balance between the metal coordination site and amyloid folding upon complexation.

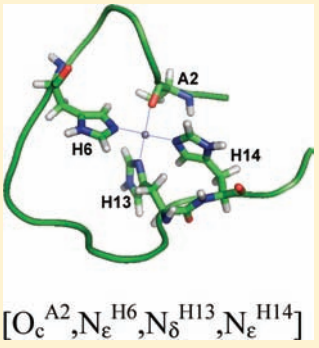

$[O_c^{A2},N_\varepsilon^{H6},N_\delta^{H13},N_\varepsilon^{H14}]$

INTRODUCTION

Alzheimer's disease (AD) is the most common form of neurodegenerative dementia.[1] It is characterized by structural changes in the brain that generate a progressive loss of neuronal abilities, and its hallmarks are intracellular neurofibrillary tangles and extracellular senile plaques.[2,3] These plaques are formed by the aggregation of amyloid-β peptide (Aβ)[4,5] and are believed to contribute to the formation of reactive oxygen species (ROS) and progressive neuronal death.[6,7]

The main alloforms of Aβ found in brain plaques are 40 and 42 amino acids long, with the Aβ42 being the least soluble and the one that displays enhanced neurotoxicity.[3] Analysis of post-mortem brain tissues shows high concentrations (∼mM) of transition metal ions such as Fe^{3+}, Cu^{2+}, and Zn^{2+} in AD plaques, thereby suggesting that Aβ aggregation could be mediated by some of these essential ions.[8] Indeed, in vitro studies revealed that these metal cations promote Aβ aggregation,[9−12] with the deposits formed being solubilized by metal chelators.[13,14] On the other hand, there is evidence that the interaction of Aβ with redox active metal ions such as Cu^{2+} can lead to the formation of reactive oxygen species (ROS).[7,15] This oxidative damage typifies AD neuropathology[16] and precedes Aβ deposition in AD.[6,17] The mechanism for the reduction of Cu^{2+} is still unclear, but some investigations suggest that Met35 or Tyr10 is involved in the electron transfer and some evidence indicates that they can be oxidized during the process.[18,19] Excellent reviews on the chemistry of Alzheimer's disease and on the role of metal ions have recently been published.[20−22]

Elucidation of the coordination of metal ions to Aβ is essential to understand their role in the aggregation of Aβ and in the production of ROS. Moreover, in-depth knowledge of the coordination environment of Cu^{2+} in Cu^{2+}-Aβ is of great importance for a rational design of new chelators with potential therapeutic applications, an increasing active area of research.[23−30] For this reason, in the last 10 years, several studies have focused their attention in determining the coordination properties of Cu^{2+} interacting with Aβ.[31−42] Earlier electron paramagnetic resonance (EPR) and nuclear magnetic resonance (NMR) experiments on Cu^{2+}-Aβ(1−28) at physiological pH revealed a square planar configuration for Cu^{2+} with most probably a 3N1O coordination sphere around the metal and with His6, His13, and His14 involved.[33] On the basis of a previous Raman spectroscopic study by Miura et al.,[38] the O ligand was assigned to the hydroxyl group of Tyr10. Several pieces of subsequent experimental evidence, however, indicate that the involvement of Tyr10 is very unlikely.[36,37,39,41] Viles et al., using a range of complementary spectroscopic techniques including circular dichroism (CD), EPR, and NMR, assigned a 4N coordination involving the three histidines and the N-terminus at pH = 7.4, and deprotonated amide nitrogens at higher pH.[41] Extended

Received: April 13, 2011
Published: August 15, 2011

dx.doi.org/10.1021/ja203407v | J. Am. Chem. Soc. 2011, 133, 15008–15014

X-ray absorption fine structure (EXAFS) studies for Cu^{2+}-Aβ-(1−16) at pH = 7.4 suggest a distorted six-coordinated mode (3N3O) including three histidines, glutamic and/or aspartic acid, and an axial water.[40] More recent studies by means of continuous wave electron paramagnetic resonance (CW-EPR) spectroscopy and hyperfine sublevel correlation (HYSCORE) have provided support for a 3N1O coordination sphere in Cu^{2+}-Aβ-(1−16).[34,35,42] At pH = 6.3−6.9 this coordination sphere arises from the binding of the terminal amino group, His6 and His13 (or His14) and an O atom from the Asp1,[35,42] whereas at pH = 8 coordination is due to the three histidines and the carbonyl group of Ala2.[34] Finally, recent EPR studies indicate that at pH = 9 only one His along with the NH_2 terminus, the amide nitrogen of Ala2, and a carbonyl oxygen are equatorial ligands of Cu^{2+}.[42] Overall, all these studies appear to indicate that the coordination environment of Cu^{2+} in soluble Cu^{2+}-Aβ complexes is highly sensitive to pH and that several distinct coordination modes involving histidine, NH_2 terminus, or amide N atoms, as well as carbonyl or carboxylate O atoms, can coexist in equilibrium.

Several theoretical studies have addressed the coordination of Cu^{2+} interacting with Aβ.[43−48] However, quantum chemical calculations with hybrid functionals, which are essential to properly describe Cu^{2+} coordination,[49] have only been applied to small model systems,[43,44,48] without accounting for the role of the peptide conformation on the metal coordination. Larger systems including the whole Aβ have been considered through classical molecular dynamic simulations[32,45,46] and, thus, without explicitly introducing the subtle electronic effects of Cu^{2+}, although one of them includes structural variables of the first coordination sphere of the metal through restrictions obtained by quantum mechanical calculations.[45] On the other hand, Carr Parrinello molecular dynamics simulations with the nonhybrid PBE functional have also been performed for simplified models of Cu^{2+}-Aβ(1−14),[47] but no firm conclusions could be drawn from these simulations.

In this study, we combine homology modeling (HM) techniques with quantum based approaches (QM) to determine plausible models for Cu^{2+}-Aβ(1−16), one of the systems for which Cu^{2+} coordination has been mostly studied experimentally but for which no X-ray or NMR data has been provided. The models obtained were energetically evaluated by means of full quantum chemical calculations which provided information on the factors that determine the stability of the complex. Despite the fact that several coordination environments have been proposed, we decided to start our study with a model that includes His6, His13, and His14 in the coordination sphere because (i) the experimentally resolved analogue Zn^{2+}-Aβ-(1−16) complex shows this kind of coordination and (ii) it is one of the most accepted proposals at physiological (or slightly larger) pH.[33,35]

COMPUTATIONAL METHODS

Model Systems. Full geometry optimizations and harmonic frequency calculations of the different small model systems in gas phase were carried out using the hybrid BHandHLYP[50,51] density functional with the standard 6-311++G(d,p) basis set for C, O, N, and H and the Watcher's (15s11p6d1f)/[10s7p4d1f] basis set for Cu.[52,53] We chose the BHandHLYP functional because previous studies in our group[49,54,55] for open shell Cu^{2+} (d^9) complexes have demonstrated that functionals with ∼50% of exact exchange provide good results compared to the highly correlated CCSD(T) method. This is due to the fact that GGA or functionals with small percentages of exact exchange such as B3LYP overstabilize too delocalized situations, as a result of a bad cancellation of the self-interaction part by the exchange-correlation functional.[56,57]

Solvation effects were modeled through single-point energy calculations at the same level of theory, with water as solvent, using the self-consistent field polarizable continuum model, (SCRF=CPCM)[58] as implemented in Gaussian 03.[59] In order to improve the thermodynamic changes of the processes under investigation, we have considered the experimental value for the solvation free energy of water (ΔG_{solv}= −6.3 kcal mol^{-1}).[60] The entropy obtained in gas phase was converted from 1 atm to 1 M by subtracting R ln(24.46) cal K^{-1} mol^{-1}. Also the term RT ln(55.6) was added to the water solvation free energy, where 55.6 M corresponds to the concentration of pure liquid water. Since in the Aβ environment the residue side chains that coordinate copper do not have the free range of motion because of the restriction imposed by the protein secondary structure, the rotational and translational entropies were removed according to the procedure used by Rickard et al.[43] Calculations of net atomic charges and spin densities were carried out using the natural population analysis (NPA).[61] All calculations for open shell systems were done considering the unrestricted formalism. Model systems include three imidazole molecules coordinated to Cu^{2+} as well as two different candidates containing oxygen as fourth ligands: CH_3COO^- and NH_2CHO. CH_3COO^- was used to model the side chain from glutamates and aspartates, and NH_2CHO was used to simulate the peptidic bonds present in the peptide.

Cu^{2+}-Aβ(1−16) Complexes. Homology modeling (HM) techniques are widely used in biochemistry and pharmacology to generate three-dimensional models of proteins of unknown structure (*target*) from analogues whose structures have been experimentally resolved (*template*), based on the idea that the highest the sequence similarity between two proteins, the highest their structural similarity.[62] Three dimensional models of the target are generated by first constructing its backbone and then performing conformational searches of the entire bunch of its side chains. The best structural models are those with lowest energy, although, in some cases, several structural features can also be considered to detect the best possible candidate(s).[63] Like most force field techniques, HM approaches are not optimized for dealing with metal ions, even less for transition metals with subtle electronic features like those of copper. However, simulating the impact of the metal ions on the structure of the target is feasible by including data obtained from external analysis (e.g., QM calculations) as additional constraints in the HM process.

Our HM calculations were performed by using the conformation of Aβ in Zn^{2+}-Aβ(1−16) as template (PDB code 1ZE9)[64] and including the geometry restraints (distances and angles) deduced from DFT calculations on small copper complexes representing the metal binding site. We selected this template because it was obtained under similar conditions to those in which copper should bind amyloid with three N atoms in the first coordination sphere. At this point, it should be noticed that the only possible pitfall of our approach would be that the backbone organization in the Cu^{2+}-Aβ complex is significantly different from that in Zn^{2+}-Aβ. Indeed, the homology modeling procedure could not reproduce correctly such reorganization at the moment. However, several pieces of experimental evidence show that this phenomenon is most unlikely. In particular, the experimental structures of free β-amyloid and Zn^{2+}-Aβ complex show very little conformational changes of the scaffold of the peptide; in the zinc bound structure, the coordination of the metal results essentially from the rearrangement of the side chains of the peptide with respect to its unbound form. A similar behavior is expected for Cu^{2+}.

HM simulations were carried out with the Modeler 9v8 package.[65] Both δ and ε coordination of all histidines (6, 13, and 14) as well as the coordination of different possible candidates containing oxygen as

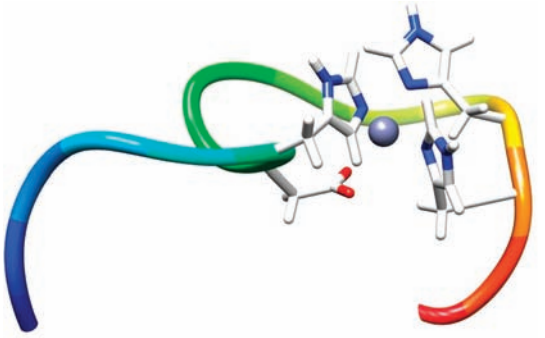

Figure 1. Example of one of the ONIOM partitions used to optimize the Cu^{2+}-Aβ(1−16) complexes. Atoms in ball and stick fashion represent the QM layer, and the rest of the atoms correspond to the MM layer.

Scheme 1. Protocol Used for the Construction and Evaluation of Cu^{2+}-Aβ(1-16) Models

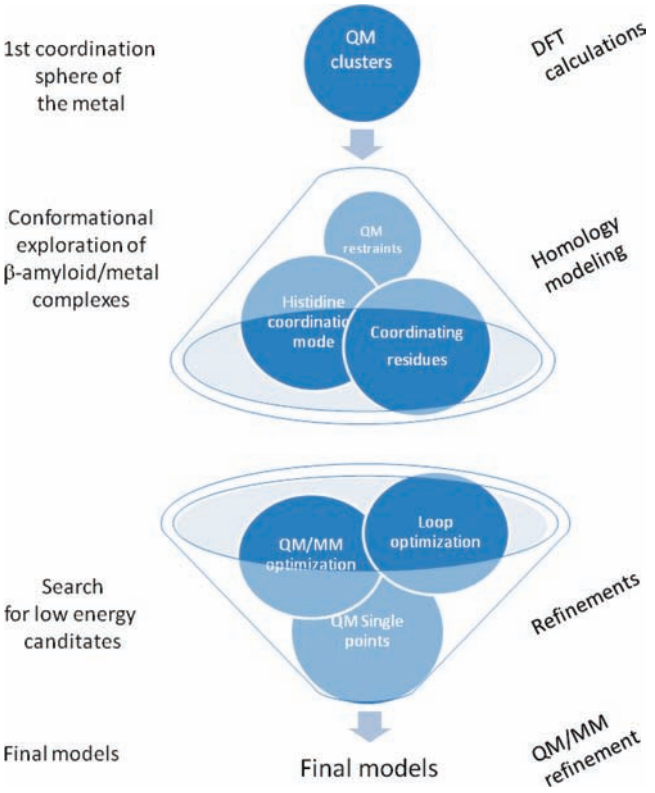

fourth ligand (Asp1, Glu3, Asp7, Glu11, and CO_{Ala2}) were tested. To select the best initial model for QM/MM (quantum mechanics/molecular mechanics) refinements, the following criterion has been considered. For each type of coordination, 500 homology models were generated, leading to a total of 20,000 hypothetical candidates for the Cu^{2+}-Aβ(1−16) complexes. The models for each configuration were grouped using the Ensemble Cluster option implemented in Chimera 1.5.2.[66] For each run, we used the *NMRclust* approach developed by Sutcliffe et al.[67] and available in UCSF Chimera. This method automatically determines the convenient cutoff values for cluster generations, avoiding the possible pitfalls of fixed rmsd cutoff values. The rmsd threshold is determined for each run. For all 500 models of a given configuration, the most representative model of the most populated

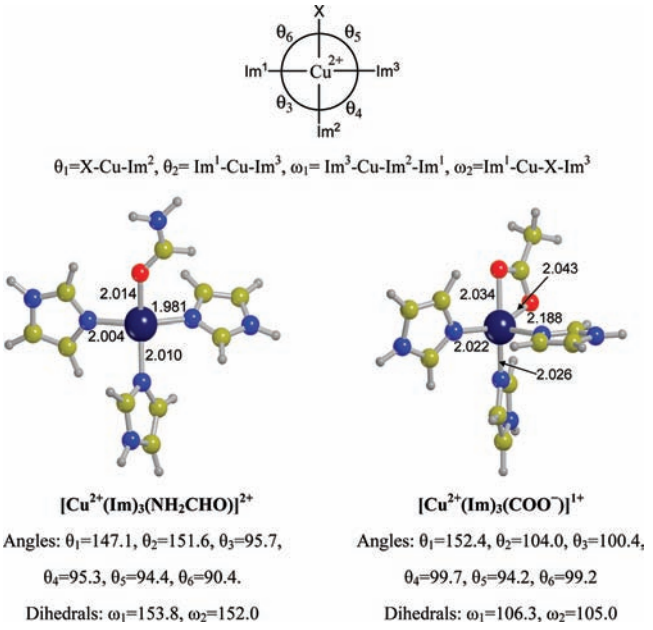

Figure 2. BHandHLYP optimized geometries for $CuIm_3X$ complexes. Distances are given in angstroms, and angles are in degrees.

clusters was selected. The clusters with low population have been discarded. Both Charmm[68] energies and Discrete Optimized Protein Energy (DOPE) score,[69] implemented in Modeler 9v8, were considered on the selected candidates. Generally, both scoring functions agree, but in the rare cases of disagreement, the best model was determined by visual inspection, taking into account structural knowledge and coordination rules. Yet, these models do not include the electronic structure effects on the metal binding site of the whole system. Therefore, these candidates were thereafter fully optimized with the ONIOM (BHandHLYP:UFF) QM/MM procedure implemented in Gaussian 03.[59] QM partition included copper atom and imidazoles from histidines 6, 13, and 14 and the lateral side chain from the candidate ligand to occupy the fourth coordination site (see Figure 1). For the QM partition the BHandHLYP[50,51] hybrid functional in combination with the Lanl2dz pseudopotential and its associated basis set for copper, and the standard 6-31G(d) basis set for the rest of atoms, was used. This basis set will be referred to hereafter as SB (small basis). The Universal Force Field (UFF)[70] was selected for the MM partition. The link atoms approach was considered to define the boundary conditions. These optimizations were done for the complex in gas phase, and thus, residues were considered in their neutral form. Otherwise, optimizations were driven by strong electrostatic interactions between negative and positive charged residues, which led to the complete loss of the secondary structure of the peptide backbone obtained from HM simulations. Moreover, single-point calculations of the amyloid without copper were carried out, at the same level of theory, in order to account for the relative stability of their secondary structures. Additionally, and with the aim of further improving the accuracy of the results, single-point energy calculations with a larger basis set (Lanl2dz and its associated basis set for copper and the standard 6-31+G(d,p) for the rest of the atoms, hereafter referred to as LB) were performed. Scheme 1 shows schematically the procedure used for the generation and evaluation of the different models.

RESULTS AND DISCUSSION

Model Systems. $[Cu^{2+}(Im)_3X]$ complexes, with X equal to CH_3COO^- and NH_2CHO and with Im being imidazole, were

chosen to study the coordination environment of Cu^{2+} interacting with three histidines and with an O ligand. We considered CH_3COO^- to represent the aspartates/glutamates coordination and NH_2CHO to simulate the coordination of a carbonyl group from the backbone. Fully optimized complexes are shown in Figure 2. It can be observed that $[Cu^{2+}(Im)_3(NH_2CHO)]^{2+}$ shows a distorted square-planar coordination, a common configuration in Cu^{2+} complexes, whereas $[Cu^{2+}(Im)_3(CH_3COO^-)]^{1+}$ exhibits a square-pyramid pentacoordination, with both oxygen atoms from the carboxylate group in equatorial positions and one imidazole in the axial position. This last coordination is similar to that found by Viles et al. by using a range of complementary spectroscopic techniques.[41] The geometrical parameters obtained from these models (distances and angles) were used afterward as restraints to build the HM models as described in the next section.

Preference for one ligand or another was evaluated by computing the energy of the $[Cu^{2+}(Im)_3(H_2O)] + X \rightarrow [Cu^{2+}(Im)_3X] + H_2O$ reaction in aqueous solution. Detailed values for these calculations are presented in the Supporting Information (SI). The computed aqueous free energies are −20.4 and −9.5 kcal mol^{-1} for CH_3COO^- and NH_2CHO, respectively, and thus clearly indicate a preference of Cu^{2+} for the CH_3COO^- group over NH_2CHO, as expected due to its negative charge.

Cu^{2+}-Aβ(1−16) Complexes. Initial models for Cu^{2+}-Aβ(1−16) were generated from HM calculations, as described in the Computational Methods section, and then relaxed with the ONIOM (BHandHLYP:UFF) QM/MM procedure. Geometry restraints (distances and angles) in the HM process are those obtained from our previous DFT calculations on small copper complexes (see Figure 2). Results (geometries and energies) for all generated complexes are given in the SI. First of all, it should be noticed that the peptide backbone after QM/MM refinement shows only minor modifications compared to the HM initial models. Moreover, metal ligand distances remain similar to those found in the small QM cluster models; that is, Cu^{2+}−O and Cu^{2+}−N distances are around 1.9−2.1 Å and 2.0−2.2 Å, respectively. However, the coordination environment differs depending on the model. For instance, for most complexes enclosing a carboxylate in its coordination sphere (17 among 32) Cu^{2+} shows distorted square pyramid pentacoordination with COO^- interacting in a bidentate fashion, a result closely similar to the one observed in the Zn^{2+}-Aβ complex[64] and in a X-ray absorption spectroscopy study of Cu^{2+}-Aβ.[40] In nine other models, the coordination with COO^- is monodentate, leading to distorted square planar environments. In these latter cases, stabilizing hydrogen bond interactions between the more distant O atom of the carboxylate and the nitrogen of the nitrogenated ligands (azole nitrogen of histidines or peptide NH groups) are observed, indicating that bi(mono)dentate coordination of COO^- is dictated by interactions with nearby residues. A similar behavior is observed in the $(H_2O)_3Cu^{2+}-CH_3COO^-$ model system, which shows a H-bond between coordinated water and the distant O atom of COO^-.[43] Interestingly, in a few cases, the relaxation of the Cu^{2+}-Aβ structure leads to a tricoordinated metal environment in which the interaction with the carboxylate is lost. This behavior has been correlated both to an excessive stress of the backbone in satisfying the constraints imposed during the HM process as well as to changes in the electronic state of the metal during the QM/MM relaxation, with both phenomena being strongly related. In these configurations, the Cu^{2+} cation is reduced to Cu^+, the spin density value on the metal cation is close to 0, and the population analysis indicates that the radical character moves to the carboxylic group initially interacting with the metal cation. Models enclosing CO_{Ala2} as fourth ligand show a unique distorted square planar tetracoordination geometry with slight deviations depending on the model considered. With respect to the preference for δ or ε coordination of histidines, no clear trends are observed.

Among the 32 models that enclose COO^- as the fourth ligand, the lowest energy structures obtained after single point BHandHLYP calculations at the fully optimized BHandHLYP:UFF geometries have the following coordination spheres: $[O^{E3}, N_\delta{}^{H6}, N_\varepsilon{}^{H13}, N_\varepsilon{}^{H14}]$ (**1**), $[O^{E3}, N_\delta{}^{H6}, N_\delta{}^{H13}, N_\delta{}^{H14}]$ (**2**), and $[O^{D7}, N_\varepsilon{}^{H6}, N_\delta{}^{H13}, N_\delta{}^{H14}]$ (**3**). The relative energies of these structures with the small basis set are 0, 14.0, and 13.0 kcal mol^{-1}, respectively, whereas the other 29 complexes are more than 30 kcal mol^{-1} less stable. With the larger basis set, the relative energies of **1**, **2**, and **3** decrease to 0, 2.6, and 4.2 kcal mol^{-1}, respectively. Inclusion of thermal effects computed at the ONIOM level does not significantly modify these values, with the relative Gibbs energies being 0, 1.4, and 2.1 kcal mol^{-1}, respectively. The structure of these three models is shown in Figure 3, and the main geometrical parameters are given in Table 1. In structure **1**, Cu^{2+} is pentacoordinated, with the carboxylate group of Glu3 interacting with the metal site in a bidentate manner. The geometry of the coordination site corresponds to a distorted trigonal bipyramid structure with O_1 and N^{H13} in the axial positions. Interaction with O_2 is weaker, and thus, the Cu−O_2 distance is around 0.2 Å larger than the Cu−O_1 one. In **2**, the interaction with the carboxylate occurs also with Glu3, but in a monodentate fashion, and the resulting geometry corresponds to a distorted square planar configuration of the metal. Finally, in **3**, the carboxylate interaction is bidentate but with Asp7. In this case, the geometry of the coordination site resembles more a square pyramidal structure with His6 in the apical position. Thus, the Cu−N^{H6} distance is around 0.2 Å larger than the ones corresponding to Cu−N^{H13} and Cu−N^{H14}.

Quantum chemical calculations for the model system (i.e., $Cu^{2+}(Im)_3CH_3COO^-$), at the same geometry as that obtained in models **1**, **2**, and **3**, indicate that the preferred coordination is the one displayed in **2**, with metal coordination in **3** and **1** being less stable by 6 and 8 kcal mol^{-1}, respectively. Thus, the energetic order of these cluster models is **2** < **3** < **1**. Nevertheless, calculations for neutral Aβ(1−16) at the geometry of **1**, **2**, and **3** show that the energetic order of amyloid in the three models is **1** < **2** < **3**. In this regard, it should be noticed that the analysis of structures **1**, **2**, and **3** revealed different hydrogen bond contacts between amide NH and CO groups of the peptide backbone as well as between side chains of different residues. Thus, the final relative stability results from a fine-tuning between both subparts of the complex.

The coordination environment of Cu^{2+} in the most stable models that contain CO_{Ala2} is nearly square planar, with Cu−O and Cu−N distances being similar or slightly shorter than those obtained in the three complexes previously described. The amyloid peptide in these configurations is, however, less stable than it is in **1**, **2**, and **3**, mainly due to the lack of NH···CO contacts. Since this observation was unexpected, additional modeling with finer refinement of the amyloid loop (from His6 to His13) was performed, but the same tendency was observed. The most stable model, $[O_c{}^{A2}, N_\varepsilon{}^{H6}, N_\delta{}^{H13}, N_\varepsilon{}^{H14}]$ (**4**), is shown in Figure 3, and its main geometry features are included in Table 1.

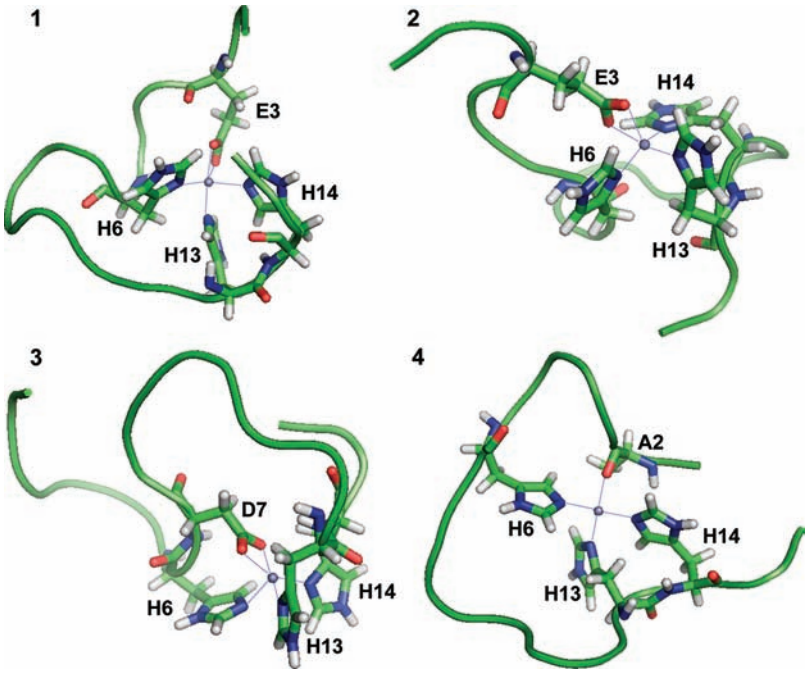

Figure 3. Most stable models enclosing COO^- (**1**, **2**, and **3**) and CO (**4**) as fourth ligand.

Table 1. Main Geometrical Parameters of the Cu^{2+} Coordination Site in the Most Stable Models Containing COO^- and CO_{Ala2} as Fourth Ligand[a]

	COO^-			CO_{Ala2}
	1	**2**	**3**	**4**
$Cu-N^{H6}$	2.04	2.06	2.20	1.98
$Cu-N^{H13}$	2.01	2.06	2.01	2.03
$Cu-N^{H14}$	2.12	2.02	2.03	1.97
$Cu-O_1$	1.98	1.99	2.04	2.00
$Cu-O_2$	2.20	2.40	2.11	
$N^{H6}-Cu-N^{H14}$	123.9	152.7	103.6	170.9
$N^{H13}-Cu-O_1$	169.9	154.0	149.9	169.1

[a] Distances are in angtroms, and angles are in degrees.

Unfortunately, direct comparison between models **1**, **2**, **3** enclosing COO^-, and **4** containing CO is not possible in gas phase because their global charges are different (+1 in **1**, **2**, and **3** and +2 in **4**). Note that in **1**, **2**, and **3** glutamate is coordinated to the metal cation while in **4** it is exposed to the solvent. Thus, in order to overcome this limitation and to provide an estimation of the relative stability of these two kinds of coordinations, we have performed continuum solvent calculations on complexes **1** and **4**, with Glu3 unprotonated in the latter. Thermal corrections were estimated from frequency calculations of these models in gas phase using the ONIOM (BHandHLYP/SB:UFF) procedure. For consistency, in these calculations the QM partition includes Ala2 main chain fragment, Glu3, and the three histidine side chains. To estimate the thermal corrections of the unprotonated complex enclosing CO, we removed the contributions associated to the hydrogen atom in Glu3. As expected, results show that solvation energy is significantly more stabilizing in **4** than in **1**. As a result, relative Gibbs energies in solution indicate that **4** is more stable by about 12 kcal mol^{-1}, suggesting that solvation effects can counterbalance the preference of the copper to bind glutamate against backbone carbonyls. This is in agreement with the results recently obtained experimentally by CW-EPR spectroscopy and hyperfine sublevel correlation (HYSCORE) in combination with ^{15}N and ^{13}C labeling, which unambiguously identify the carbonyl oxygen of Ala2 as the fourth oxygen ligand in a complex with three histidines in the coordination sphere (component II).[34]

CONCLUSIONS

In this study, we combine homology modeling (HM) techniques with quantum based approaches (QM) to determine three-dimensional models for Cu^{2+}-Aβ(1−16) with three histidines in the coordination sphere. We considered both ε and δ coordination of histidines 6, 13, and 14 as well as the coordination of different possible candidates containing oxygen as the fourth ligand (Asp1, Glu3, Asp7, Glu11, and CO_{Ala2}). Among the 32 models that enclose COO^-, the lowest energy structures correspond to $[O^{E3},N_\delta{}^{H6},N_\varepsilon{}^{H13},N_\varepsilon{}^{H14}]$ (**1**), $[O^{E3},N_\delta{}^{H6},N_\delta{}^{H13},N_\delta{}^{H14}]$ (**2**), and $[O^{D7},N_\varepsilon{}^{H6},N_\delta{}^{H13},N_\delta{}^{H14}]$ (**3**), whereas the most stable model containing CO_{Ala2} in the Cu^{2+} coordination sphere is $[O_c{}^{A2},N_\varepsilon{}^{H6},N_\delta{}^{H13},N_\varepsilon{}^{H14}]$ (**4**). An estimation of the relative stability between Glu3 (**1**) and CO_{Ala2} (**4**) coordinated complexes seems to indicate that the preference for the latter coordination may be due to solvent effects.

These models offer a unique framework for understanding the factors that drive copper-Aβ interactions at a molecular level, which should provide major insights in the design of new AD therapeutic agents as well as an understanding of the mechanism of ROS formation. Moreover, our results highlight the synergic relationship between the peptidic and metallic moieties in defining the overall geometry of the complex and illustrate that the final stability of the complexes results from a balance between the metal coordination site and amyloid folding upon complexation. This synergy can lead to different coordinations of the metal

in a 3N1O fashion that are energetically close and could play a role in physiological conditions. Finally, it is to be noticed that the integrative computational approaches used in the present study, and that combine QM and HM techniques, have allowed deepening into a fundamental phenomenon that requires both a conformational exploration and the modeling of fine electronic effects. This study newly illustrates the potential of such approaches[71] in decoding key molecular events involving metal binding processes.

■ ASSOCIATED CONTENT

Supporting Information. Cartesian coordinates of the 40 final models and tables containing primary data for all calculations. Complete references for refs 7, 13, 59, and 68. This material is available free of charge via the Internet at http://pubs.acs.org.

■ AUTHOR INFORMATION

Corresponding Author
mariona.sodupe@uab.cat jeandidier.marechal@uab.cat.

■ ACKNOWLEDGMENT

The authors gratefully acknowledge financial support from MICINN through the CTQ2008-06381/BQU, CTQ2008-06866-C02-01, and CSD2007-00006 projects and the use of computer time at the CESCA supercomputing center. J.A.-T. acknowledges the MICINN for the provision of the graduate studentship BES-2007-14304.

■ REFERENCES

(1) http://www.alz.org/alzheimers_disease_facts_figures.asp.
(2) Hardy, J.; Selkoe, D. J. *Science* **2002**, *297* (5580), 353–356.
(3) Selkoe, D. J. *Physiol. Rev.* **2001**, *81* (2), 741–766.
(4) Glenner, G. G.; Wong, C. W. *Biochem. Biophys. Res. Commun.* **1984**, *120* (3), 885–890.
(5) Masters, C. L.; Simms, G.; Weinman, N. A.; Multhaup, G.; McDonald, B. L.; Beyreuther, K. *Proc. Natl. Acad. Sci.* **1985**, *82* (12), 4245–4249.
(6) Bush, A. I. *Neurosciences* **2003**, *26* (4), 207–214.
(7) Huang, X. D.; et al. *J. Biol. Chem.* **1999**, *274* (52), 37111–37116.
(8) Lovell, M. A.; Robertson, J. D.; Teesdale, W. J.; Campbell, J. L.; Markesbery, W. R. *J. Neurol. Sci.* **1998**, *158* (1), 47–52.
(9) Bush, A. I.; Pettingell, W. H.; Multhaup, G.; Paradis, M. d.; Vonsattel, J.-P.; Gusella, J. F.; Beyreuther, K.; Masters, C. L.; Tanzi, R. E. *Science* **1994**, *265* (5177), 1464–1467.
(10) Atwood, C. S.; Moir, R. D.; Huang, X.; Scarpa, R. C.; Bacarra, N. M. E.; Romano, D. M.; Hartshorn, M. A.; Tanzi, R. E.; Bush, A. I. *J. Biol. Chem.* **1998**, *273* (21), 12817–12826.
(11) Mantyh, P. W.; Ghilardi, J. R.; Rogers, S.; Demaster, E.; Allen, C. J.; Stimson, E. R.; Maggio, J. E. *J. Neurochem.* **1993**, *61* (3), 1171–1174.
(12) Esler, W. P.; Stimson, E. R.; Jennings, J. M.; Ghilardi, J. R.; Mantyh, P. W.; Maggio, J. E. *J. Neurochem.* **1996**, *66* (2), 723–732.
(13) Cherny, R. A.; et al. *Neuron* **2001**, *30* (3), 665–676.
(14) Cherny, R. A.; Legg, J. T.; McLean, C. A.; Fairlie, D. P.; Huang, X. D.; Atwood, C. S.; Beyreuther, K.; Tanzi, R. E.; Masters, C. L.; Bush, A. I. *J. Biol. Chem.* **1999**, *274* (33), 23223–23228.
(15) Opazo, C.; Huang, X.; Cherny, R. A.; Moir, R. D.; Roher, A. E.; White, A. R.; Cappai, R.; Masters, C. L.; Tanzi, R. E.; Inestrosa, N. C.; Bush, A. I. *J. Biol. Chem.* **2002**, *277* (43), 40302–40308.
(16) Dong, J.; Atwood, C. S.; Anderson, V. E.; Siedlak, S. L.; Smith, M. A.; Perry, G.; Carey, P. R. *Biochemistry* **2003**, *42* (10), 2768–2773.
(17) Nunomura, A.; Perry, G.; Aliev, G.; Hirai, K.; Takeda, A.; Balraj, E. K.; Jones, P. K.; Ghanbari, H.; Wataya, T.; Shimohama, S.; Chiba, S.; Atwood, C. S.; Petersen, R. B.; Smith, M. A. *J. Neuropath. Exp. Neur.* **2001**, *60* (8), 759–767.
(18) Barnham, K. J.; Haeffner, F.; Ciccotosto, G. D.; Curtain, C. C.; Tew, D.; Mavros, C.; Beyreuther, K.; Carrington, D.; Masters, C. L.; Cherny, R. A.; Cappai, R.; Bush, A. I. *FASEB J.* **2004**, *18* (12), 1427–1429.
(19) Butterfield, D. A.; Kanski, J. *Peptides* **2002**, *23* (7), 1299–1309.
(20) Rauk, A. *Chem. Soc. Rev.* **2009**, *38* (9), 2698–2715.
(21) Faller, P. *ChemBioChem* **2009**, *10* (18), 2837–2845.
(22) Faller, P.; Hureau, C. *Dalton Trans.* **2009**, *7*, 1080–1094.
(23) Liu, G.; Men, P.; Perry, G.; Smith, M. A. *Free Radicals and Antioxidant Protocols*, 2nd ed.; pp 123−144.
(24) Folk, D. S.; Franz, K. J. *J. Am. Chem. Soc. 132*, (14), 4994−4995.
(25) Rodriguez-Rodriguez, C.; de Groot, N. S.; Rimola, A.; Alvarez-Larena, A.; Lloveras, V.; Vidal-Gancedo, J.; Ventura, S.; Vendrell, J.; Sodupe, M.; Gonzalez-Duarte, P. *J. Am. Chem. Soc.* **2009**, *131* (4), 1436–1451.
(26) Scott, L. E.; Orvig, C. *Chem. Rev.* **2009**, *109* (10), 4885–4910.
(27) Hindo, S. S.; Mancino, A. M.; Braymer, J. J.; Liu, Y. H.; Vivekanandan, S.; Ramamoorthy, A.; Lim, M. H. *J. Am. Chem. Soc.* **2009**, *131* (46), 16663–16665.
(28) Wu, W. H.; Lei, P.; Liu, Q.; Hu, J.; Gunn, A. P.; Chen, M. S.; Rui, Y. F.; Su, X. Y.; Xie, Z. P.; Zhao, Y. F.; Bush, A. I.; Li, Y. M. *J. Biol. Chem.* **2008**, *283* (46), 31657–31664.
(29) Hureau, C.; Saaki, I.; Gras, E.; Faller, P. *ChemBioChem* **2010**, *11* (7), 950–953.
(30) Rodríguez-Rodríguez, C.; Rimola, A.; Alí-Torres, J.; Sodupe, M.; Gonzalez-Duarte, P. *J. Comput.-Aided Mol. Des.* **2011**, *25*, 21–30.
(31) Hou, L. M.; Zagorski, M. G. *J. Am. Chem. Soc.* **2006**, *128* (29), 9260–9261.
(32) Parthasarathy, S.; Long, F.; Miller, Y.; Xiao, Y.; McElheny, D.; Thurber, K.; Ma, B.; Nussinov, R.; Ishii, Y. *J. Am. Chem. Soc.* **2011**, *133* (10), 3390–3400.
(33) Curtain, C. C.; Ali, F.; Volitakis, I.; Cherny, R. A.; Norton, R. S.; Beyreuther, K.; Barrow, C. J.; Masters, C. L.; Bush, A. I.; Barnham, K. J. *J. Biol. Chem.* **2001**, *276* (23), 20466–20473.
(34) Drew, S. C.; Masters, C. L.; Barnham, K. J. *J. Am. Chem. Soc.* **2009**, *131* (25), 8760–8761.
(35) Drew, S. C.; Noble, C. J.; Masters, C. L.; Hanson, G. R.; Barnham, K. J. *J. Am. Chem. Soc.* **2009**, *131* (3), 1195–1207.
(36) Guilloreau, L.; Damian, L.; Coppel, Y.; Mazarguil, H.; Winterhalter, M.; Faller, P. *J. Biol. Inorg. Chem.* **2006**, *11* (8), 1024–1038.
(37) Karr, J. W.; Akintoye, H.; Kaupp, L. J.; Szalai, V. A. *Biochemistry* **2005**, *44* (14), 5478–5487.
(38) Miura, T.; Suzuki, K.; Kohata, N.; Takeuchi, H. *Biochemistry* **2000**, *39* (23), 7024–7031.
(39) Streltsov, V. *Eur. Biophys. J. Biophys.* **2008**, *37* (3), 257–263.
(40) Streltsov, V. A.; Titmuss, S. J.; Epa, V. C.; Barnham, K. J.; Masters, C. L.; Varghese, J. N. *Biophys. J.* **2008**, *95* (7), 3447–3456.
(41) Syme, C. D.; Nadal, R. C.; Rigby, S. E. J.; Viles, J. H. *J. Biol. Chem.* **2004**, *279* (18), 18169–18177.
(42) Dorlet, P.; Gambarelli, S.; Faller, P.; Hureau, C. *Angew. Chem., Int. Ed.* **2009**, *48* (50), 9273–9276.
(43) Rickard, G. A.; Gomez-Balderas, R.; Brunelle, P.; Raffa, D. F.; Rauk, A. *J. Phys. Chem. A* **2005**, *109* (37), 8361–8370.
(44) Hewitt, N.; Rauk, A. *J. Phys. Chem. B* **2009**, *113* (4), 1202–1209.
(45) Mantri, Y.; Fioroni, M.; Baik, M. H. *J. Biol. Inorg. Chem.* **2008**, *13* (8), 1197–1204.
(46) Raffa, D. F.; Rauk, A. *J. Phys. Chem. B* **2007**, *111* (14), 3789–3799.
(47) Minicozzi, V.; Morante, S.; Rossi, G. C.; Stellato, F.; Christian, N.; Jansen, K. *Int. J. Quantum Chem.* **2008**, *108* (11), 1992–2015.
(48) Marino, T.; Russo, N.; Toscano, M.; Pavelka, M. *Interdiscip. Sci.: Comput. Life Sci.* **2010**, *2*, 57–69.
(49) Rios-Font, R.; Sodupe, M.; Rodriguez-Santiago, L.; Taylor, P. R. *J. Phys. Chem. A* **2010**, *114* (40), 10857–10863.
(50) Becke, A. D. *J. Chem. Phys.* **1993**, *98* (2), 1372–1377.

(51) Lee, C.; Yang, W.; Parr, R. G. *Phys. Rev. B* **1988**, *37* (2), 785–789.
(52) Hay, P. J. *J. Chem. Phys.* **1977**, *66* (10), 4377–4384.
(53) Wachters, A. J. H. *J. Chem. Phys.* **1970**, *52* (3), 1033–1036.
(54) Rimola, A.; Rodriguez-Santiago, L.; Sodupe, M. *J. Phys. Chem. B* **2006**, *110* (47), 24189–24199.
(55) Georgieva, I.; Trendafilova, N.; Rodriguez-Santiago, L.; Sodupe, M. *J. Phys. Chem. A* **2005**, *109* (25), 5668–5676.
(56) Poater, J.; Sola, M.; Rimola, A.; Rodriguez-Santiago, L.; Sodupe, M. *J. Phys. Chem. A* **2004**, *108* (28), 6072–6078.
(57) Sodupe, M.; Bertran, J.; Rodriguez-Santiago, L.; Baerends, E. J. *J. Phys. Chem. A* **1999**, *103* (1), 166–170.
(58) Barone, V.; Cossi, M. *J. Phys. Chem. A* **1998**, *102* (11), 1995–2001.
(59) Frisch, M. T.; et al. *Gaussian 03*, revision D.01; 2004.
(60) Camaioni, D. M.; Schwerdtfeger, C. A. *J. Phys. Chem. A* **2005**, *109* (47), 10795–10797.
(61) Weinhold, F.; Carpenter, J. E. *The Structure of Small Molecules and Ions*; Plenum: New York, 1988.
(62) Chothia, C.; Lesk, A. M. *EMBO J.* **1986**, *5* (4), 823–826.
(63) Marti-Renom, M. A.; Stuart, A. C.; Fiser, A.; Sanchez, R.; Melo, F.; Sali, A. *Annu. Rev. Biophys. Biomed.* **2000**, *29*, 291–325.
(64) Zirah, S.; Kozin, S. A.; Mazur, A. K.; Blond, A.; Cheminant, M.; Segalas-Milazzo, I.; Debey, P.; Rebuffat, S. *J. Biol. Chem.* **2006**, *281* (4), 2151–2161.
(65) Andrej Šali, B. W.; Madhusudhan, M. S.; Shen, M. Y.; Ma, M.-R.; Narayanan Eswar, F. A.; Topf, M.; Oliva, B.; Fiser, A.; Roberto Sánchez, B. Y.; Badretdinov, A.; Francisco Melo, J. P. O.; Feyfant, E. *MODELLER A Program for Protein Structure Modeling 9v8*; 2007.
(66) Pettersen, E. F.; Goddard, T. D.; Huang, C. C.; Couch, G. S.; Greenblatt, D. M.; Meng, E. C.; Ferrin, T. E. *J. Comput. Chem.* **2004**, *25* (13), 1605–1612.
(67) Kelley, L. A.; Gardner, S. P.; Sutcliffe, M. J. *Protein Eng.* **1996**, *9* (11), 1063–1065.
(68) MacKerell, A. D.; et al. *J. Phys. Chem. B* **1998**, *102* (18), 3586–3616.
(69) Shen, M. Y.; Sali, A. *Protein Sci.* **2006**, *15* (11), 2507–2524.
(70) Rappe, A. K.; Casewit, C. J.; Colwell, K. S.; Goddard, W. A.; Skiff, W. M. *J. Am. Chem. Soc.* **1992**, *114* (25), 10024–10035.
(71) Muñoz Robles, V.; Ortega-Carrasco, E.; González Fuentes, E.; Lledós, A.; Maréchal, J.-D. *Faraday Discuss.* **2011**, *148*, 137–159.